DOE/SF/17905--T10

Thermoelectric Material Development

Quarterly Technical Progress Report

01/01/95 - 03/31/95

Jan W. Vandersande and Thierry Caillat

Jet Propulsion Laboratory/
California Institute of Technology
Pasadena, CA 91109

Technical Progress Report

Introduction

The investigation of the thermoelectric properties of n-type $Ir_xCo_{1-x}Sb_3$ solid solutions has shown that, although significant improvements compared to the binary compounds $IrSb_3$ and $CoSb_3$ were obtained, the maximum ZT value obtained was only about 0.36 at 300 C. In order to achieve significantly higher ZT values, one approach is to look at other skutterudite systems which might have thermal conductivities. The minimum thermal conductivity achieved for the $Ir_xCo_{1-x}Sb_3$ solid solutions was about 30 $mW.cm^{-1}.K^{-1}$. New ternary skutterudite compounds were discovered at JPL such as $Ru_{0.5}Pd_{0.5}Sb_3$ and $RuSb_2Te$. These compounds have shown interesting thermoelectric properties and in particular a relatively low thermal conductivity.

The objectives of the present effort is to investigate the properties of alloys of the binary compounds $IrSb_3$ and $CoSb_3$ with the ternary compound $RuSb_2Te$. $RuSb_2Te$ is a new ternary skutterudite with a room temperature thermal conductivity of about 28 $mW.cm^{-1}.K^{-1}$ (about 25% of the room temperature thermal conductivity of $IrSb_3$ and $CoSb_3$). Alloys between $IrSb_3$ and $CoSb_3$ and $RuSb_2Te$ might have significantly lower thermal conductivity than $Ir_xCo_{1-x}Sb_3$ solid solutions, resulting in better thermoelectric properties. Efforts have initially focused on determining the solubility limit of the compound in $IrSb_3$ and $CoSb_3$. The results are presented in this report. Thermoelectric properties of some on hot-pressed samples are also presented.

A. Samples preparation and characterization

Elemental powders of Ru, Sb, Te, Co and Ir (purity of 99.9% or higher) in amounts close to stoichiometric ratios were loaded inside a glove box under argon atmosphere. The loads (about 2.5 grams total weight) were placed in plastic vials

and mixed for about 15 minutes in a miller. The mixed powders were then cold - pressed in a 1/4 inch steel die under about 5-6 tons of pressure. The cold-pressed samples were then placed inside quartz ampoules, sealed under vacuum and reacted by solid state diffusion at 600 C for 5 days. The products of the reaction were then analyzed by X-ray diffractometry using the Cu-Kα line. Si powder was added to the samples as a reference.

After the X-ray diffractometry results showed that single phase powders were obtained, the samples were hot-pressed at about 600^{o}C for 2 hours in graphite dies of 6.35 mm ID at pressures of up to 20,000 psi. An *Astrot hot-pressing furnace with a constant flow of argon was used. Compact cylindrical pellets 6.4 mm in diameter and 5 to 8 mm long were obtained by this process.

The microstructure of the samples was analyzed by microprobe analysis (MPA) to assess their homogeneity and to determine if any secondary phases were present. Samples containing secondary phases were determined not to be suitable for measurements. All the samples were characterized at room temperature by Hall effect and Seebeck coefficient measurements. High temperature Hall effect, Seebeck coefficient electrical resistivity and thermal conductivity measurements were performed on selected samples.

B. $(RuSb_2Te)_x(CoSb_3)_{1-x}$ alloys

Table 1 summarizes the results obtained on $(RuSb_2Te)_x(CoSb_3)_{1-x}$ alloys. The lattice constant is 9.039 Å for $CoSb_3$ and 9.281 Å for $RuSb_2Te$. Because of the relatively large difference in lattice constant between the two compounds, one would expect that the solid solution range between the compounds will only be limited. Two samples were prepared with the following compositions: $(RuSb_2Te)_{0.125}(CoSb_3)_{0.875}$ (sample OX25) and $(RuSb_2Te)_{0.875}(CoSb_3)_{0.125}$ (sample OX26). For both samples, the X-ray pattern shows the presence of two different skutterudite phases in the samples (see Figures 1 and 2). The corresponding lattice constant is listed in Table 1 together with the corresponding percentage of the $RuSb_2Te$ phase in the sample (assuming that the lattice constant

varies linearly from one compound to the other). Based on these results, it seems like there a miscibility gap between the two compounds as shown in Figure 3. The miscibility on both sides of the system is about 5%. Sample OX46 was prepared on the basis of these results with a nominal composition with 5% of $RuSb_2Te$. The X-ray pattern shown in Figure 4 shows that the sample is essentially single phase and that the corresponding skutterudite phase has a lattice constant of 9.045 Å (~3% of $RuSb_2Te$ in $CoSb_3$). This sample was hot-pressed and its properties are shown in Table 1. The sample shows n-type conductivity with a relatively high doping level and reasonably good Hall mobility. The Seebeck coefficient values are relatively large and the electrical resistivity are relatively low, resulting in good power factor value (~ 39 $\mu W.cm^{-1}.K^{-2}$). The high temperature properties of this sample are summarized in Table 3. The Seebeck coefficient and electrical resistivity values increase with increasing temperature up to 600°C, resulting in a nearly constant power factor of about 40 $\mu W.cm^{-1}.K^{-2}$. The thermal conductivity decreases from a room temperature value of about 55 $mW.cm^{-1}.K^{-1}$ to a minimum value of about 35 $mW.cm^{-1}.K^{-1}$ at 400°C and then increases up to a value of about 42 $mW.cm^{-1}.K^{-1}$ at 600°C. The calculated ZT values are listed in Table 3 and shown in Figure 5. A maximum ZT value of 0.89 was obtained at 600°C. The values for state-of-the-art PbTe and Bi_2Te_3-based alloys are also shown in Figure 5. The values obtained for the $(RuSb_2Te)_{0.05}(CoSb_3)_{0.95}$ n-type alloy compare well with the state-of-the-art material and this is a very encouraging result. Microprobe analysis remains to be performed on this sample to investigate its composition and microstructure.

Preliminary results obtained for $(RuSb_2Te)_x(CoSb_3)_{1-x}$ alloys showed that good ZT values were obtained for n-type alloys on the $CoSb_3$-rich side. However, the ZT values are still limited because the reduction in thermal conductivity is not as important for the solid solution with about 5% of $RuSb_2Te$ as it would be for a solid solution with about 25 % of $RuSb_2Te$. Based on the results obtained so far, it seems that the miscibility limit in this system is about 5% on each side. However, longer anneals on samples containing more than 5% of one phase in the other might result in single phase, homogeneous samples. This will be investigated in the future. More samples within the solubility limit established so far will also

be prepared and their thermoelectric properties measured to confirm the good results obtained on n-type alloys.

C. $(RuSb_2Te)_x(IrSb_3)_{1-x}$ alloys

Table 2 summarizes the results obtained on $(RuSb_2Te)_x(IrSb_3)_{1-x}$ alloys. The lattice constant of $IrSb_3$ is 9.2533 Å while the lattice constant of $RuSb_2Te$ is 9.2811 Å. The difference in lattice constant is much less between $IrSb_3$ and $RuSb_2Te$ than between $CoSb_3$ and $RuSb_2Te$ and the miscibility is expected to be larger than in the system $(RuSb_2Te)_x(CoSb_3)_{1-x}$. Samples with several different compositions (listed in Table 2) were prepared and analyzed by X-ray diffractometry. The results (Figures 6-12) show that all the samples were single phase and the corresponding lattice constant are also listed in Table 2. Figure 3 shows the percentage of the $RuSb_2Te$ compound which was calculated from the lattice constant obtained from X-ray diffractometry. The results seem to indicate that a complete range of solid solutions exist between $IrSb_3$ and $RuSb_2Te$.

Samples OX5, OX5#2, OX5#3, OX6#2 and OX6#3 were all hot-pressed at temperatures higher than 750 C. Microprobe analysis showed that all these samples showed some decomposition and presence of arsenopyrite phases (higher melting point, AX_2 phases) was always detected. Measurements of the thermoelectric properties of these samples were not performed because the amount of secondary phase was too important. Samples DX1 and DX2 were hot-pressed at 700 and 600 C, respectively. Microprobe analysis of these samples showed that they were almost single phase with the skutterudite structure. The samples show p-type conductivity although they were doped with Pt which is a good n-type dopant for $IrSb_3$. The Hall mobilities are reasonably good for such alloys. The Seebeck coefficient is relatively low, typical of p-type skutterudite phases. The room temperature thermal conductivity of the $IrSb_3$-rich alloy is about 44.3 mW. $cm^{-1}.K^{-1}$ while it is about 29 $mW.cm^{-1}.K^{-1}$ for the $RuSb_2Te$-rich alloy. $IrSb_3$-rich alloys have larger thermal conductivity than $RuSb_2Te$-rich alloys which is expected because the thermal conductivity of $RuSb_2Te$ is only 25% of the value

for $IrSb_3$. Thus, better thermoelectric properties might be expected on for the $RuSb_2Te$-rich alloys. The high temperature Seebeck coefficient, electrical resistivity and power factor values are shown in Figures 13 and 14 for sample DX2 and DX1, respectively. The maximum power factor value achieved is about 6.5 $\mu W.cm^{-1}.K^{-2}$ for sample DX1 at 500 C. This is relatively low because of the relatively Seebeck coefficient values achieved for p-type skutterudite phases. N-type $RuSb_2Te$ alloys might have a much better potential because the electron effective mass is larger, resulting in larger Seebeck coefficient values. For the $(RuSb_2Te)_x(IrSb_3)_{1-x}$ alloys, efforts will now concentrate on preparation of n-type $RuSb_2Te$-rich alloys to investigate their potential. Larger amounts of platinum might produce n-type samples but other dopants such as Ni or Pd will also be investigated.

D. Summary and future work

We have found that there is a limited range of solid solutions between the skutterudite compounds $CoSb_3$ and $RuSb_2Te$ (about 5% on each side). For the system $(RuSb_2Te)_x(CoSb_3)_{1-x}$, preliminary results obtained on one n-type sample on the $CoSb_3$-rich side show that these alloys have good thermoelectric properties and a maximum ZT of about 0.89 was obtained at about 600 C. More experiments will be started to investigate the possibility of a broader range of miscibility in this system which would allow an even further decrease in the lattice thermal conductivity, resulting in better thermoelectric properties. $IrSb_3$ and $RuSb_2Te$ form a complete range of solid solutions. Hot-pressed samples in this system have shown p-type conductivity. The thermoelectric properties of these p-type alloys have been measured and results have shown that their potential for thermoelectric applications is limited mainly because of the relatively low Seebeck coefficient values for p-type materials. Efforts will be directed on preparing n-type samples of the same alloys by doping with various dopants such as Ni and Pd.

$RuSb_2Te$ - based compositions	Sample Label	Melting Point (C)	X-ray results	lattice A	% of $RuSb_2Te$	ApB g	dgeo $g.cm^{-3}$	d_{exp} $g.cm^{-3}$	d_{theo} $g.cm^{-3}$	E_{gap} eV	cc_{300} cm^{-3}	μ_{H300} cm^2/Vs	ρ_{300} $m\Omega.cm$	S_{300} $\mu V/K$	λ_{300} mW/cmK
$CoSb_3$		850		9.039	0	106.05			7.621	0.550	3.71E+18	1746.0	0.96	130.0	104
$IrSb_3$		1141		9.253		139.37			9.335	1.180	1.82E+19	1477.0	0.29	70.0	110
$RuSb_2Te$		810		9.281	100										
$Ru_{0.88}Co_7Sb_{23}Te_{1.02}$	OX 25		2 skutterudite	9.051	4.97906	107.56									
Te-rich $(CoSb_{3\ 99.875})(RuSb_2Te)_{0.125}$			phases	9.265	93.4687										
$Ru_{0.88}Co_1Sb_{17}Te_{7.02}$	OX 26		2 skutterudite	9.05	4.59763	116.56									
Te-rich $(CoSb_{3\ 99.125})(RuSb_2Te)_{0.875}$			phases	9.267	94.2316										
$Ru_{0.4}Co_{7.6}Sb_{23.6}Te_{0.4}$	OX 46		single phase	9.045	2.69053	106.65	7.512	7.534	7.648				0.91	-189.7	
$(CoSb_{3\ 99.95})(RuSb_2Te)_{0.05}$	1-OX46										1.50E+20	-32.6	1.28	-173.5	
	3-OX46										1.55E+20	-33.5	1.20	-207.8	55

Table 1: Room temperature properties of (CoSb3)x(RuSb2Te)1-x alloys

$RuSb_2Te$ - based compositions	Sample Label	Melting Point (C)	X-ray results	lattice A	ApB g	dgeo $g.cm^{-3}$	d_{wet} $g.cm^{-3}$	d_{300} $g.cm^{-3}$	E_{gap} eV	cc_{300} cm^{-3}	μ_{H300} cm^2/Vs	ρ_{300} $m\Omega.cm$	S_{300} $\mu V/K$	λ_{300} mW/cmK
$CoSb_3$		850		9.0385	106.05			7.621	0.550	3.71E+18	1746.0	0.96	130.0	104
$IrSb_3$		1141		9.2533	139.37			9.335	1.180	1.82E+19	1477.0	0.29	70.0	110
$RuSb_2Te$		810		9.2811										
$Ru_2Ir_6Sb_{22}Te_2$ $(IrSb_3)_{0.75}(RuSb_2Te)_{0.25}$	OX5	?	single phase	9.2644	134.08			8.948						
	1-OX5													
	2-OX5								1.240					
$Ru_2Ir_6Sb_{22}Te_2$ $(IrSb_3)_{0.75}(RuSb_2Te)_{0.25}$	OX5 #2	?	single phase	9.2607	134.08			8.959						
$Ru_{1.98}Ir_6Sb_{22}Te_{2.02}$ $(IrSb_3)_{0.75}(RuSb_2Te)_{0.25}$	OX5 #3	?	single phase	9.26718	134.09			8.941						
	1-OX53													
$Ru_4Ir_4Sb_{20}Te_4$ $(IrSb_3)_{0.5}(RuSb_2Te)_{0.5}$	OX6 #2		single phase	9.26718	128.78			8.587						
$Ru_{3.97}Ir_4Sb_{20}Te_{4.03}$ $(IrSb_3)_{0.5}(RuSb_2Te)_{0.5}$	OX6 #3		single phase	9.26718	128.81			8.589						
	1-OX63													
$Ru_1Ir_7Sb_{23}Te_1Pt_{0.04}$ 0.12at% Pt-doped, $(IrSb_3)_{0.875}(RuSb_2Te)_{0.125}$	DX1		single phase	9.25978	136.77	9.011		9.142				1.61	66.3	44.3
	1-DX1									1.60E+19	204.5	1.91		
	3-DX1									2.33E+19	175.2	1.53		
$Ru_{0.92}Ir_{8.02}Sb_{16}Te_7Pt_{0.16}$ 0.5at% Pt-doped, $(IrSb_3)_{0.125}(RuSb_2Te)_{0.875}$	DX2		single phase	9.2700	117.15			7.804				8.35	129.1	29.5

Table 2: Room temperature properties of (IrSb3)x(RuSb2Te)1-x alloys

T(K)	T(C)	ρ	S	PF	λ	ZT	λ_L
273	0	1.039	-203.23	39.76	57.22	0.190	52.32815
298	25	1.065	-205.69	39.74	55.24	0.214	50.03239
323	50	1.092	-208.15	39.69	53.26	0.241	47.75806
348	75	1.120	-210.61	39.61	51.28	0.269	45.50308
373	100	1.148	-213.07	39.53	49.31	0.299	43.26514
398	125	1.177	-215.53	39.45	47.33	0.332	41.04187
423	150	1.207	-217.99	39.38	45.35	0.367	38.8308
448	175	1.235	-220.45	39.33	43.66	0.404	36.9188
473	200	1.264	-223.53	39.53	42.19	0.443	35.23343
498	225	1.291	-226.86	39.85	40.90	0.485	33.7235
523	250	1.318	-230.17	40.20	39.74	0.529	32.35642
548	275	1.343	-233.26	40.52	38.71	0.574	31.11552
573	300	1.366	-235.98	40.76	37.80	0.618	29.99746
598	325	1.387	-238.23	40.91	37.03	0.661	29.00946
623	350	1.406	-239.97	40.95	36.41	0.701	28.16675
648	375	1.423	-241.19	40.89	35.96	0.737	27.48978
673	400	1.436	-241.97	40.77	35.72	0.768	27.00163
698	425	1.446	-242.42	40.64	35.70	0.795	26.72522
723	450	1.453	-242.77	40.57	35.94	0.816	26.68062
748	475	1.456	-243.35	40.68	36.44	0.835	26.88237
773	500	1.454	-244.64	41.15	37.22	0.855	27.33663
798	525	1.449	-245.93	41.75	38.28	0.870	28.03839
823	550	1.438	-247.21	42.49	39.61	0.883	28.96874
848	575	1.428	-248.50	43.25	41.18	0.891	30.13063
873	600	1.418	-249.78	44.01	42.93	0.895	31.47682

Table 3: High temperature properties of sample OX46 (see Table 1 for composition)

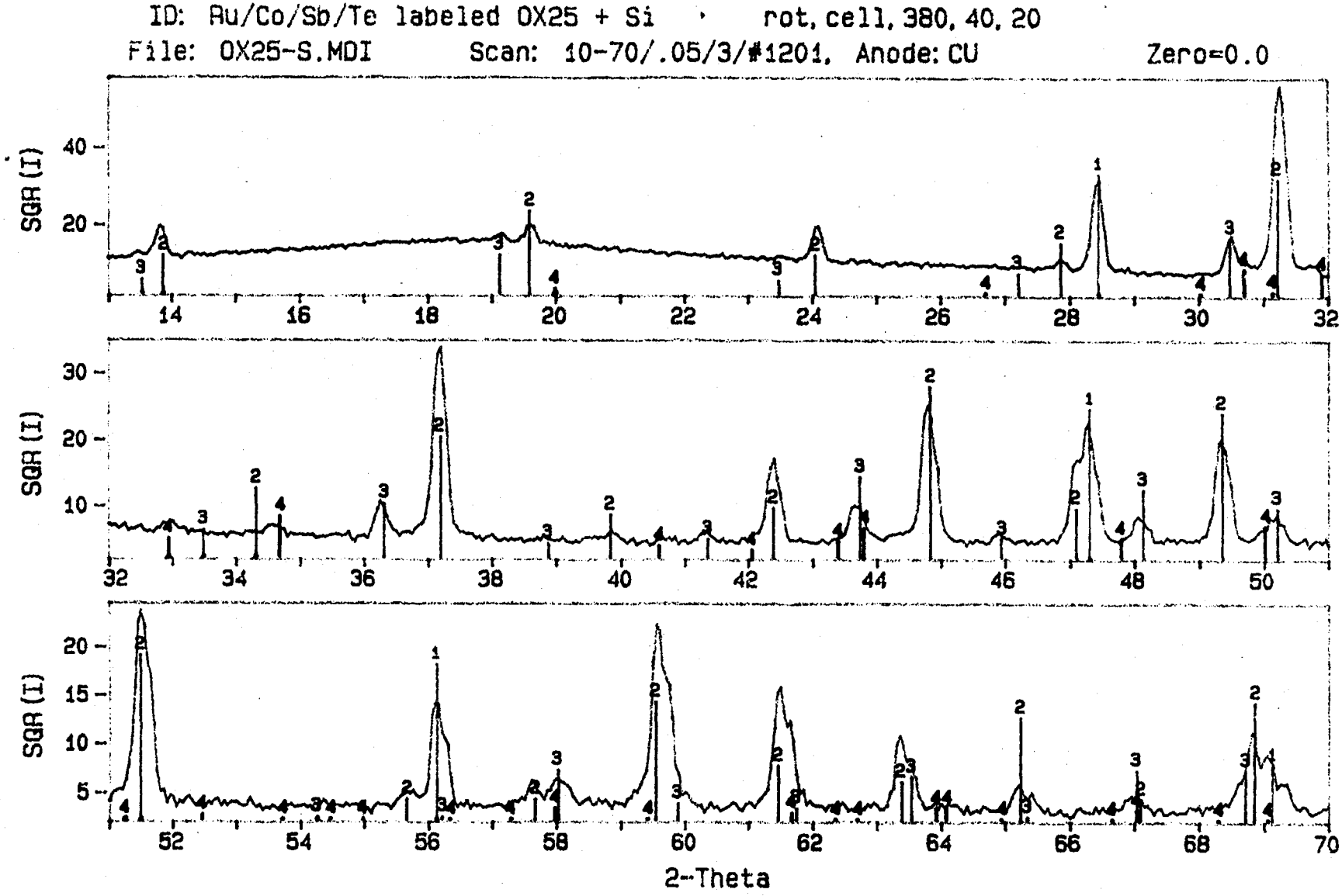
ID: Ru/Co/Sb/Te labeled OX25 + Si · rot, cell, 380, 40, 20
File: OX25-S.MDI Scan: 10-70/.05/3/#1201, Anode: CU Zero=0.0
SQR (I)
2-Theta
1> 27-1402: Silicon, syn [NR]
2> IrSb3 isostructure d/d(0)=0.9781
3> IrSb3 isostructure d/d(0)=1.0013
4> 34-0340: Antimony Ruthenium

Figure 1

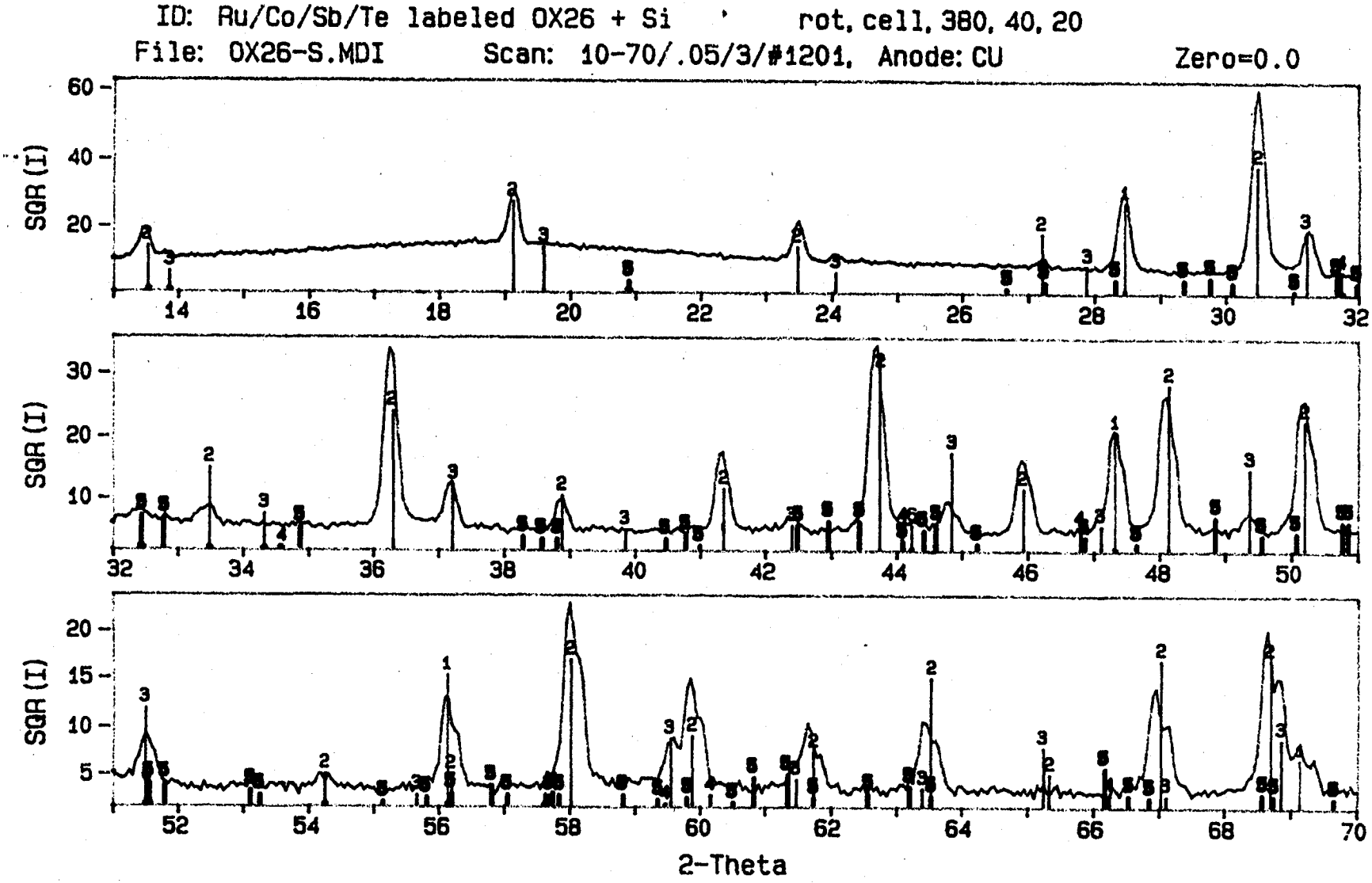

1> 27-1402: Silicon, syn [NR]

2> IrSb3 isostructure d/d(0)=1.0015

3> IrSb3 isostructure d/d(0)=0.9780

4> 33-0097: Antimony Cobalt SbCo

5> 41-1337: Ruthenium Antimony Telluride

6> 15-0806: Cobalt

RuSbTe

Figure 2

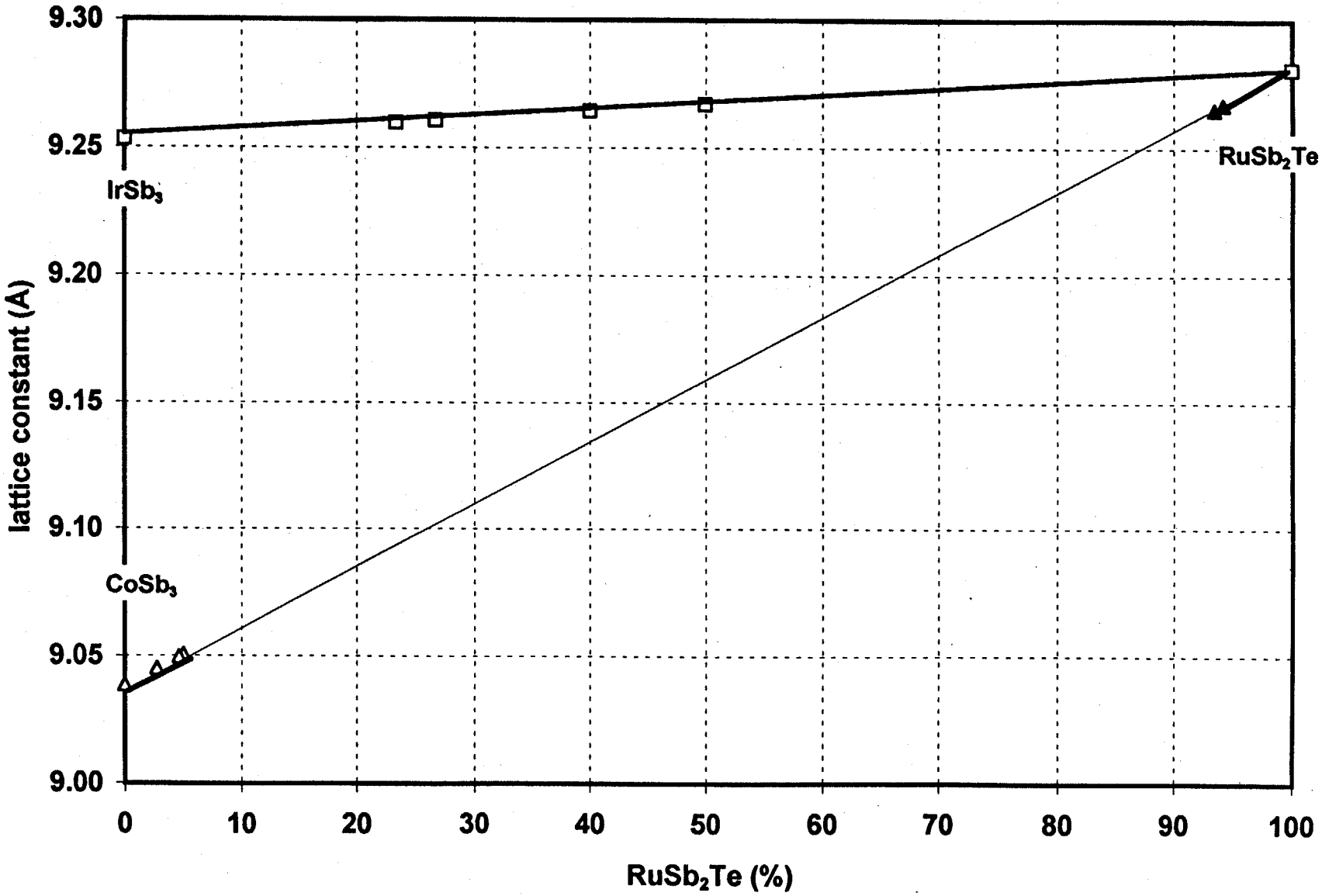

Figure 3: Lattice constant as a function of composition for (IrSb3)x(RuSb2Te)1-x and (CoSb3)x(RuSb2Te)1-x alloys

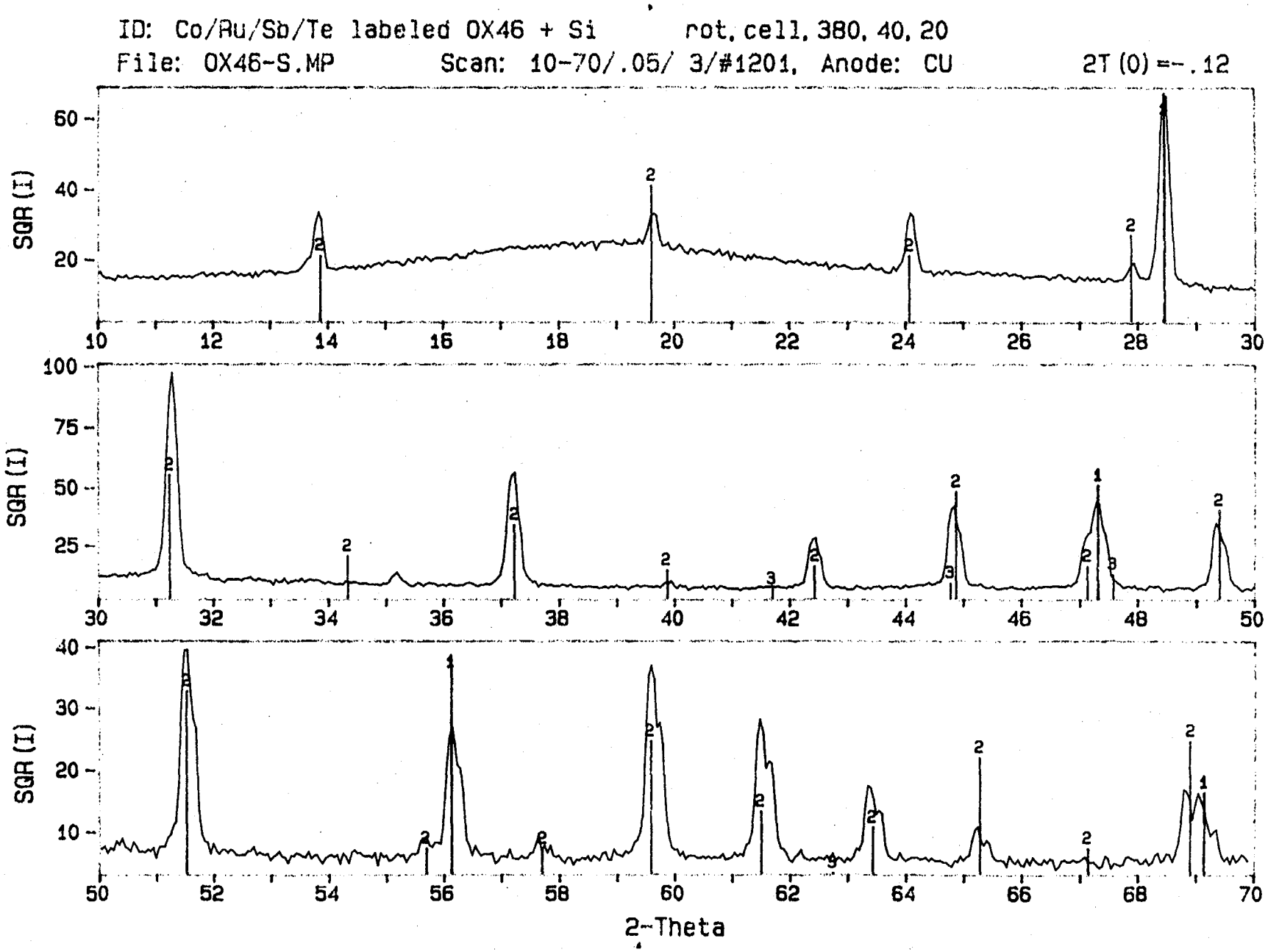
ID: Co/Ru/Sb/Te labeled OX46 + Si rot, cell, 380, 40, 20
File: OX46-S.MP Scan: 10-70/.05/ 3/#1201, Anode: CU 2T (0) =-.12
SQR (I)
2-Theta
1> 27-1402: Silicon, syn - Si
2> P17-0888, Ir Sb3, d/d (0) =.9775
3> 05-0727: Co - Cobalt

Figure 4

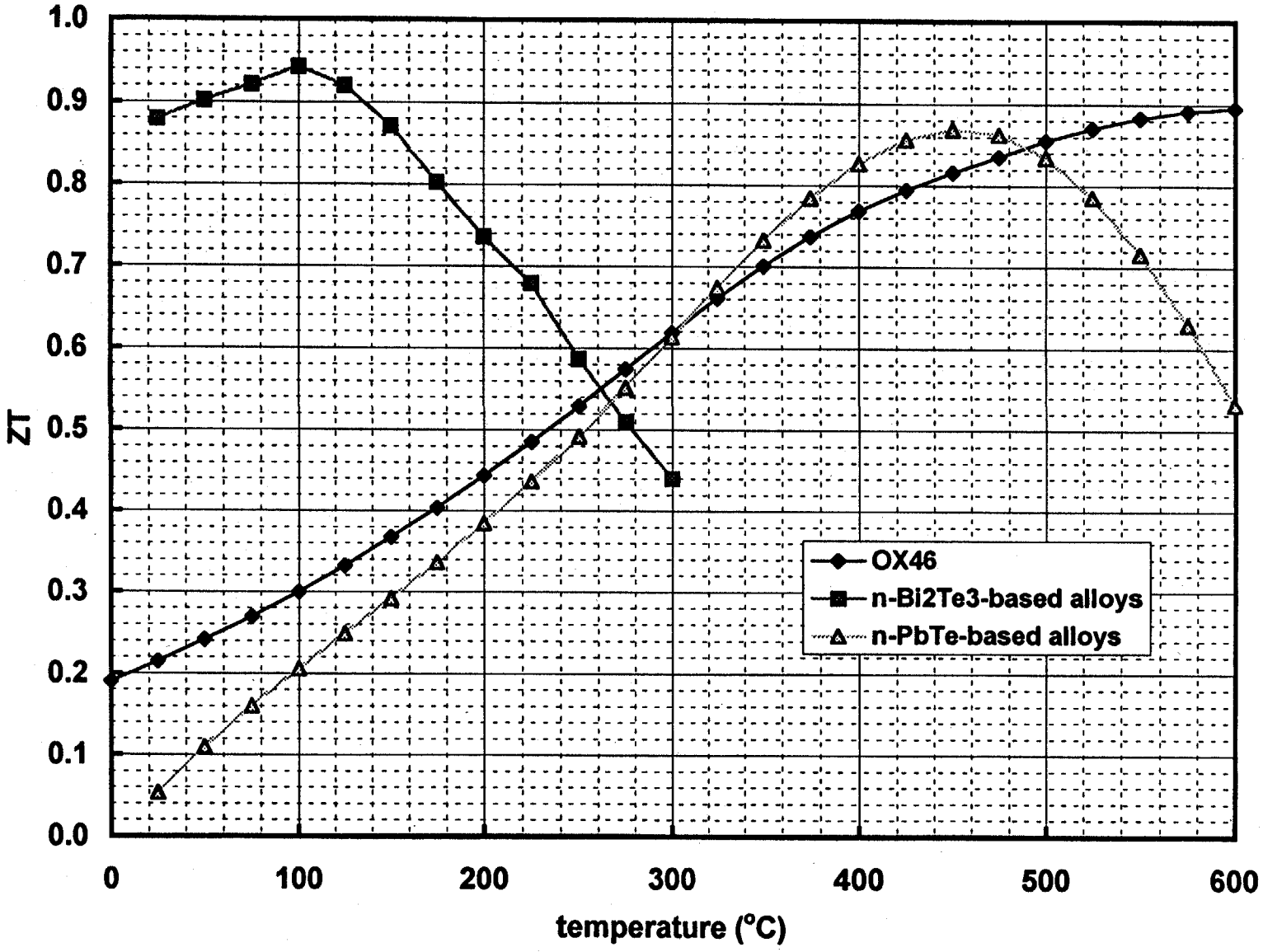

Figure 5: ZT values for sample OX46

$Ru_2Ir_6Sb_{22}Te_2$

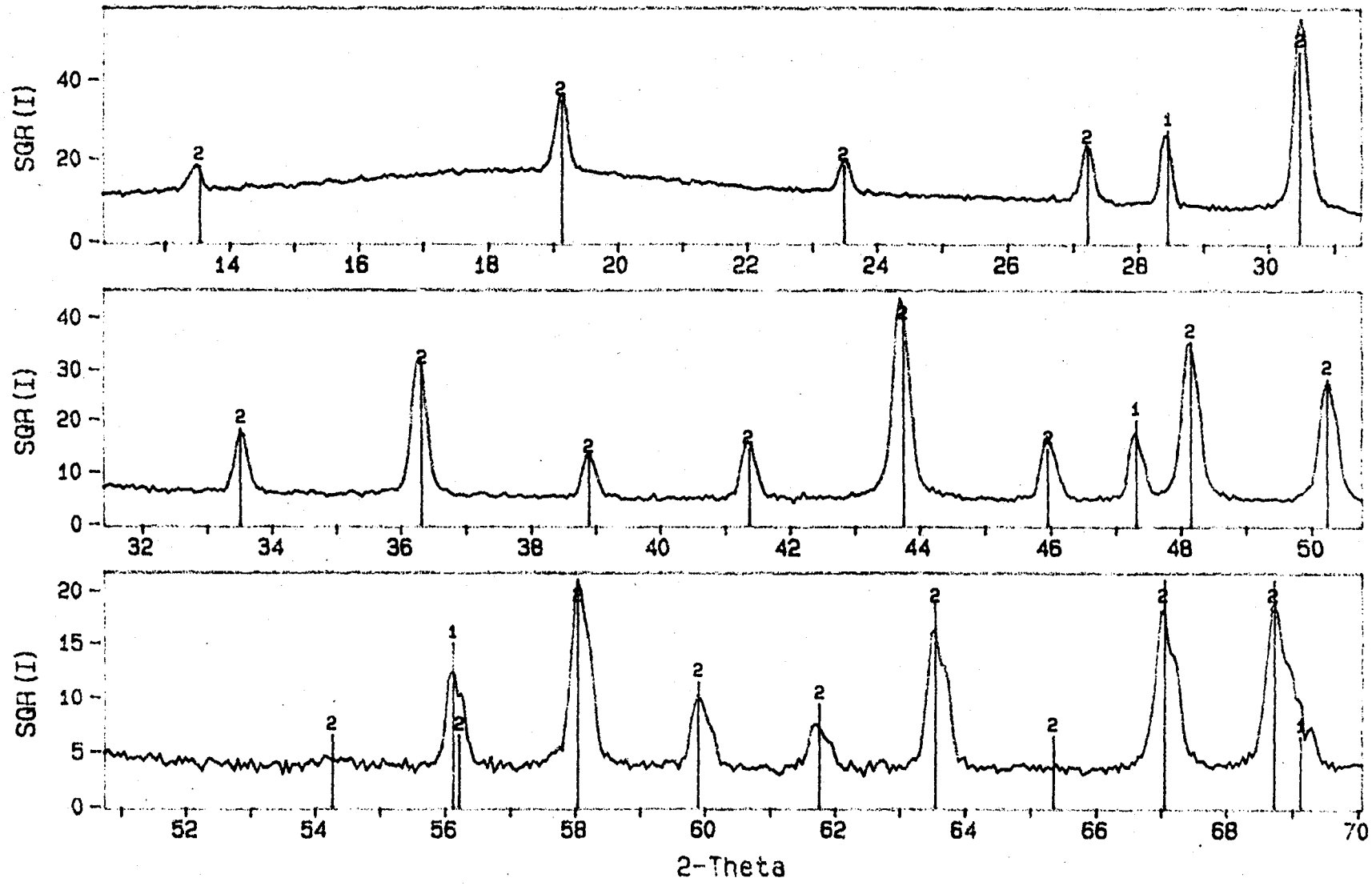

Figure 6

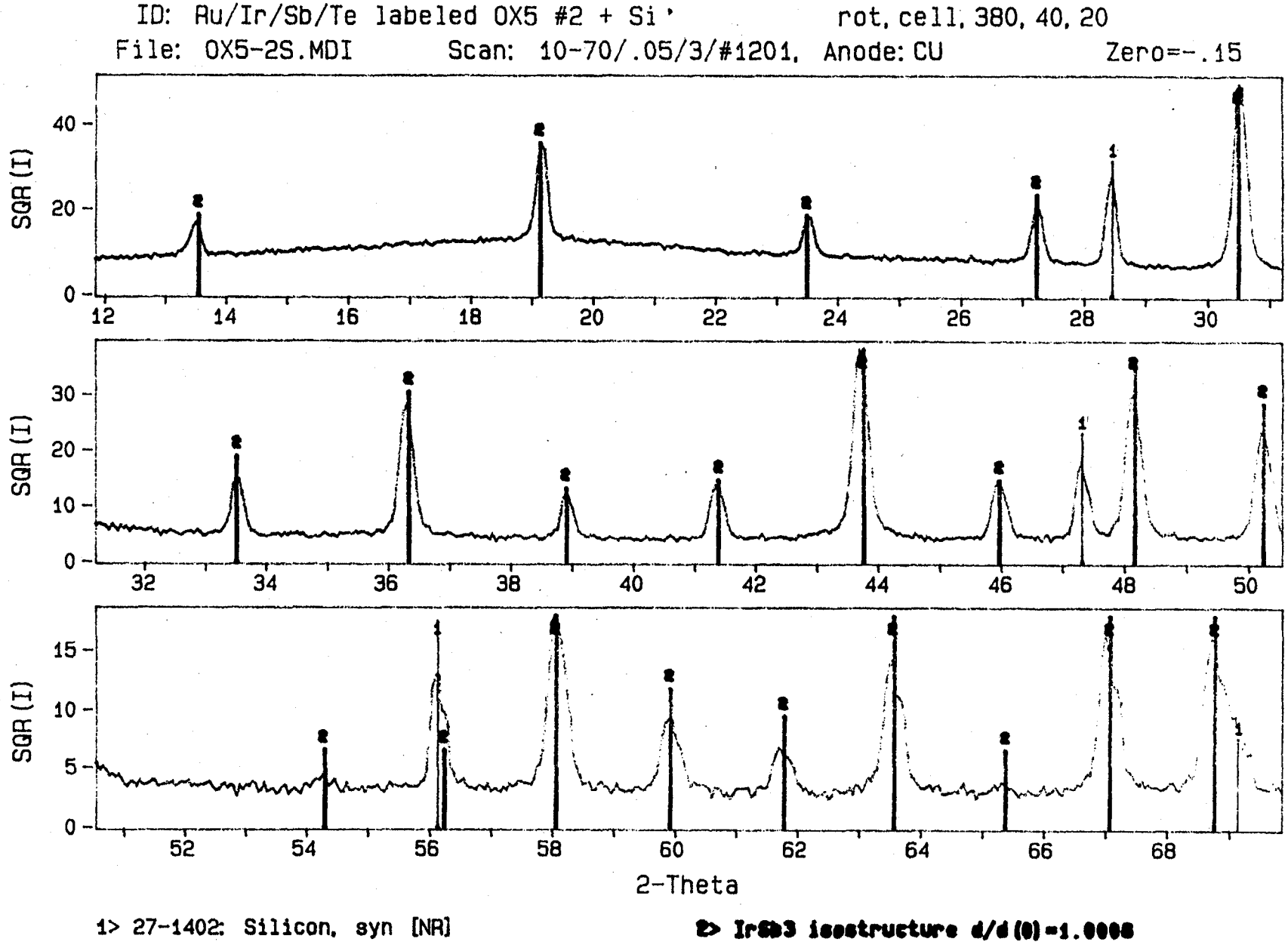
ID: Ru/Ir/Sb/Te labeled OX5 #2 + Si
rot, cell, 380, 40, 20
File: OX5-2S.MDI
Scan: 10-70/.05/3/#1201, Anode: CU
Zero=-.15
SQR(I)
2-Theta
1> 27-1402: Silicon, syn [NR]
2> IrSb3 isostructure d/d(0)=1.0008

Figure 7

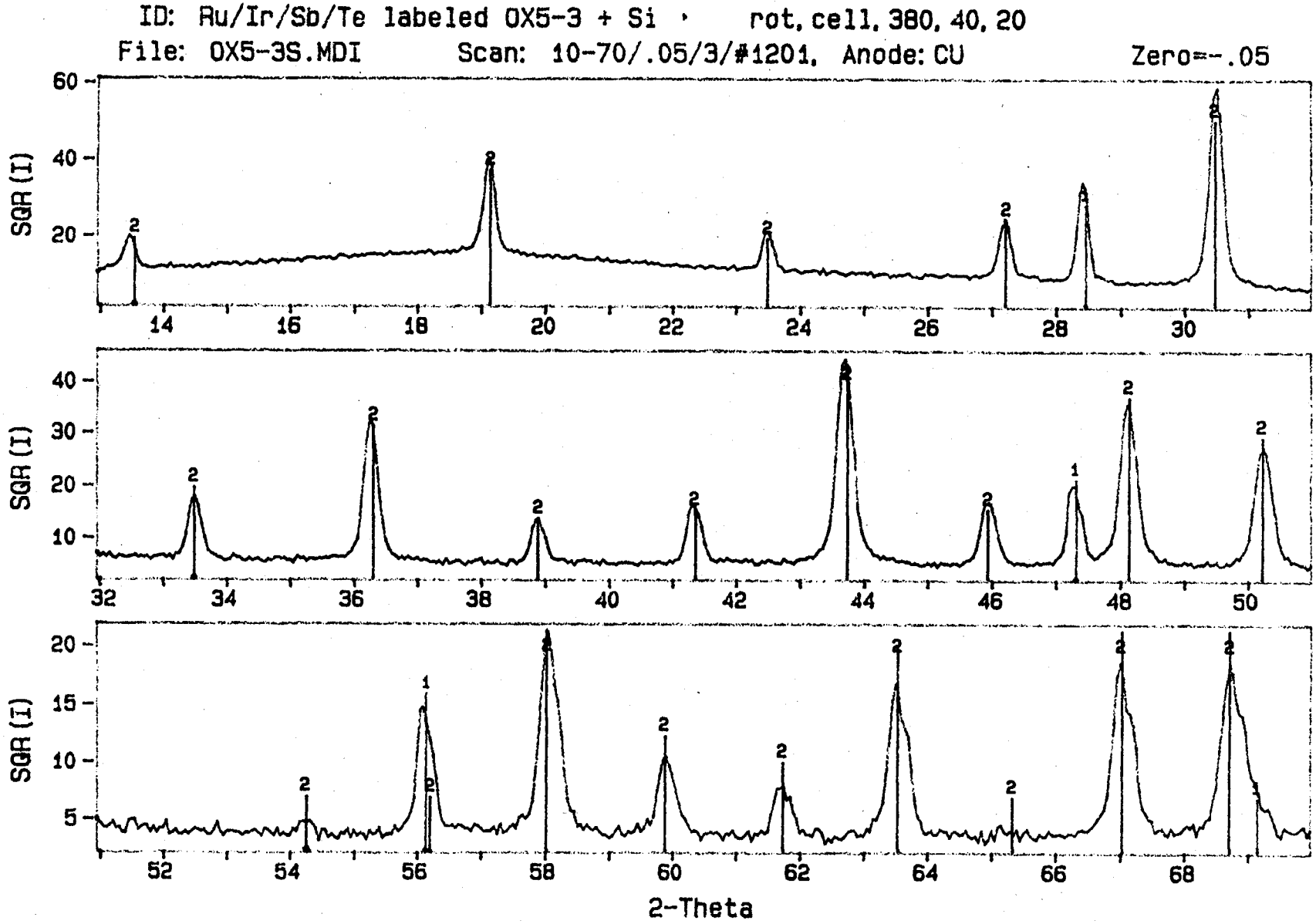
ID: Ru/Ir/Sb/Te labeled OX5-3 + Si · rot, cell, 380, 40, 20
File: OX5-3S.MDI Scan: 10-70/.05/3/#1201, Anode: CU Zero=-.05
SQR(I)
2-Theta
1> 27-1402: Silicon, syn [NR]
2> IrSb3 isostructure d/d(0)=1.0015

Figure 8

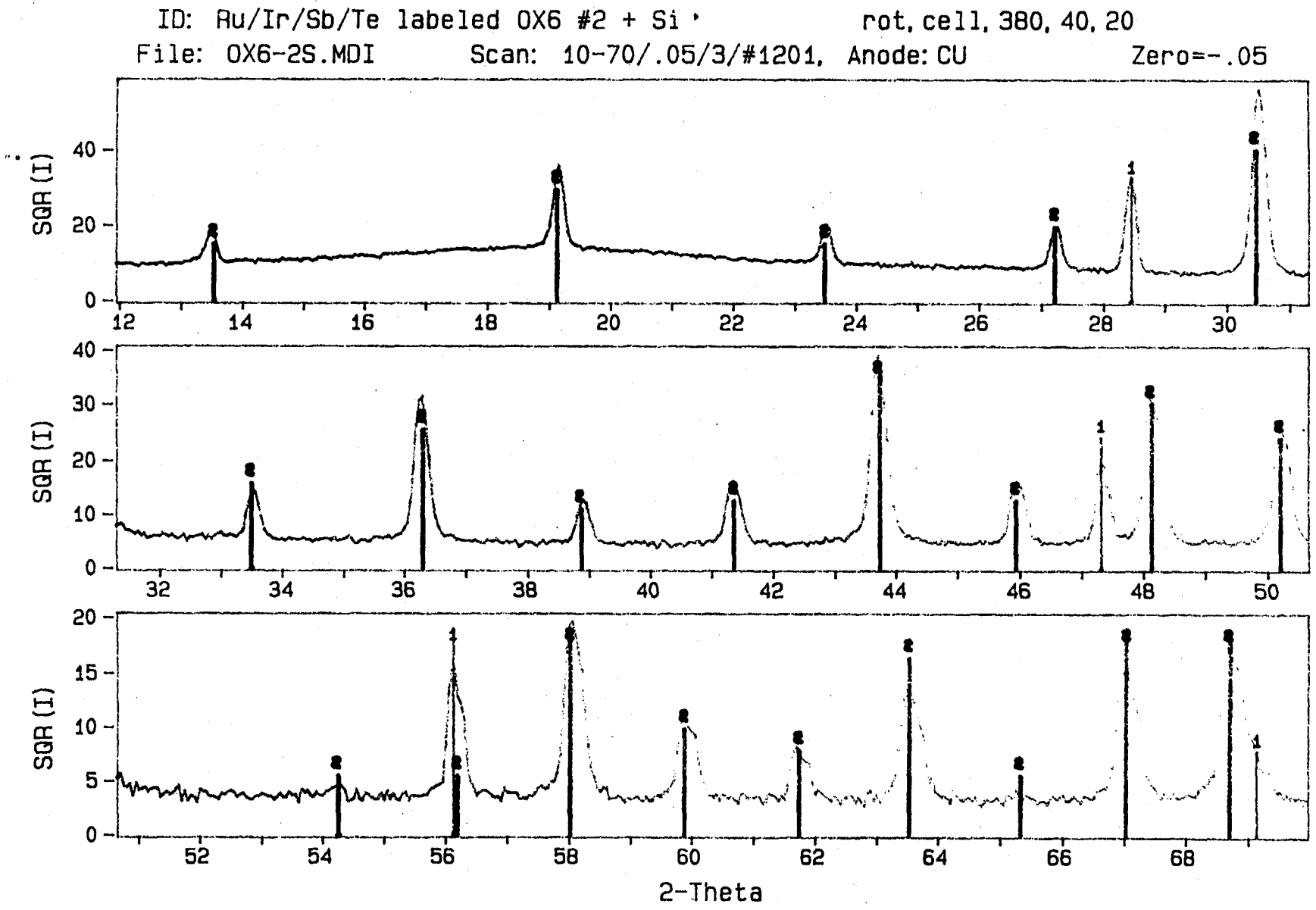
ID: Ru/Ir/Sb/Te labeled OX6 #2 + Si
rot, cell, 380, 40, 20
File: OX6-2S.MDI
Scan: 10-70/.05/3/#1201, Anode: CU
Zero=-.05
SQR(I)
2-Theta
1> 27-1402: Silicon, syn [NR]
2> IrSb3 isostructure d/d(0)=1.0015

Figure 9

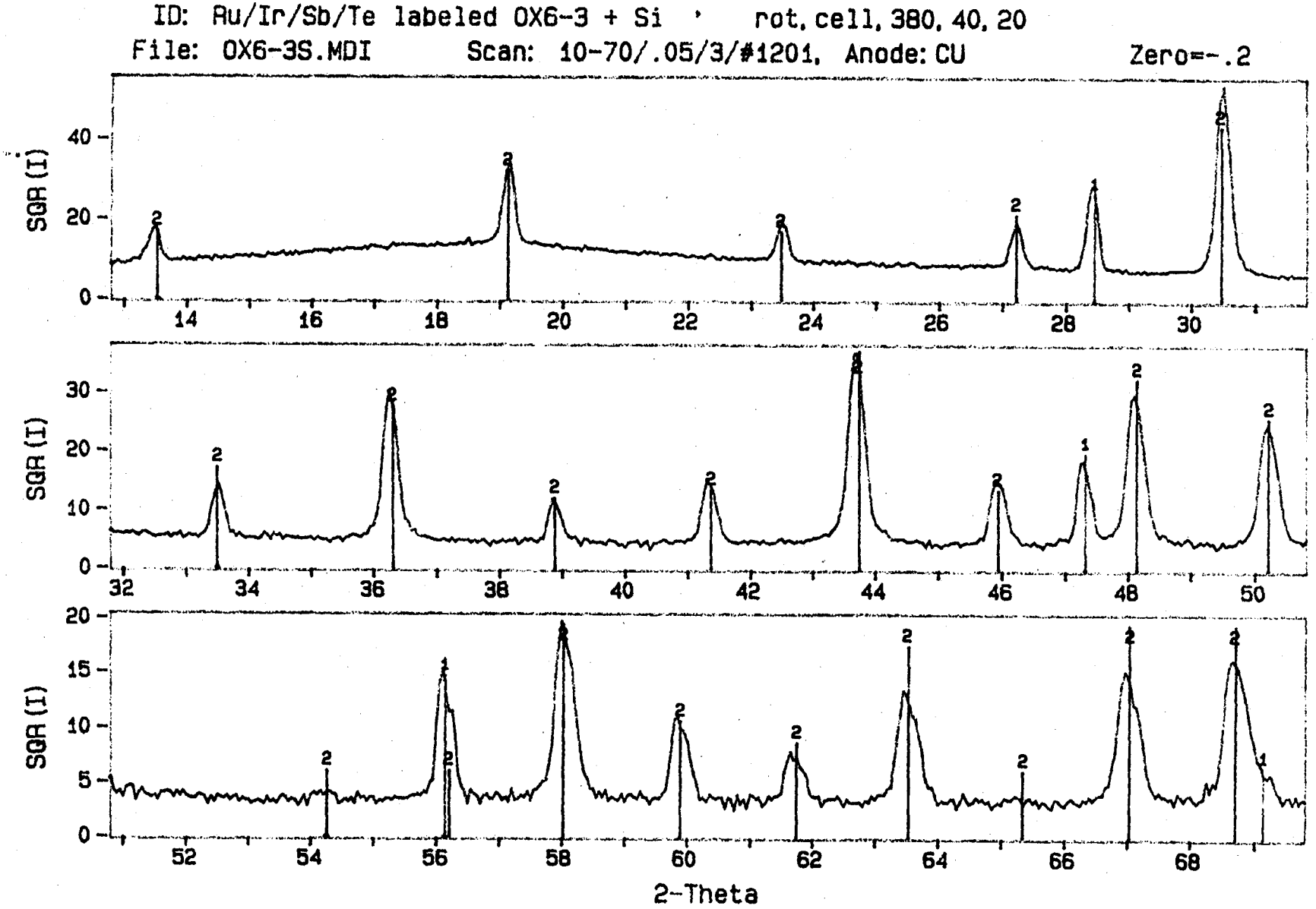
ID: Ru/Ir/Sb/Te labeled OX6-3 + Si • rot, cell, 380, 40, 20
File: OX6-3S.MDI Scan: 10-70/.05/3/#1201, Anode: CU Zero=-.2
SQR(I)
2-Theta
1> 27-1402: Silicon, syn [NR]
2> IrSb3 isostructure d/d(0)=1.0015

Figure 10

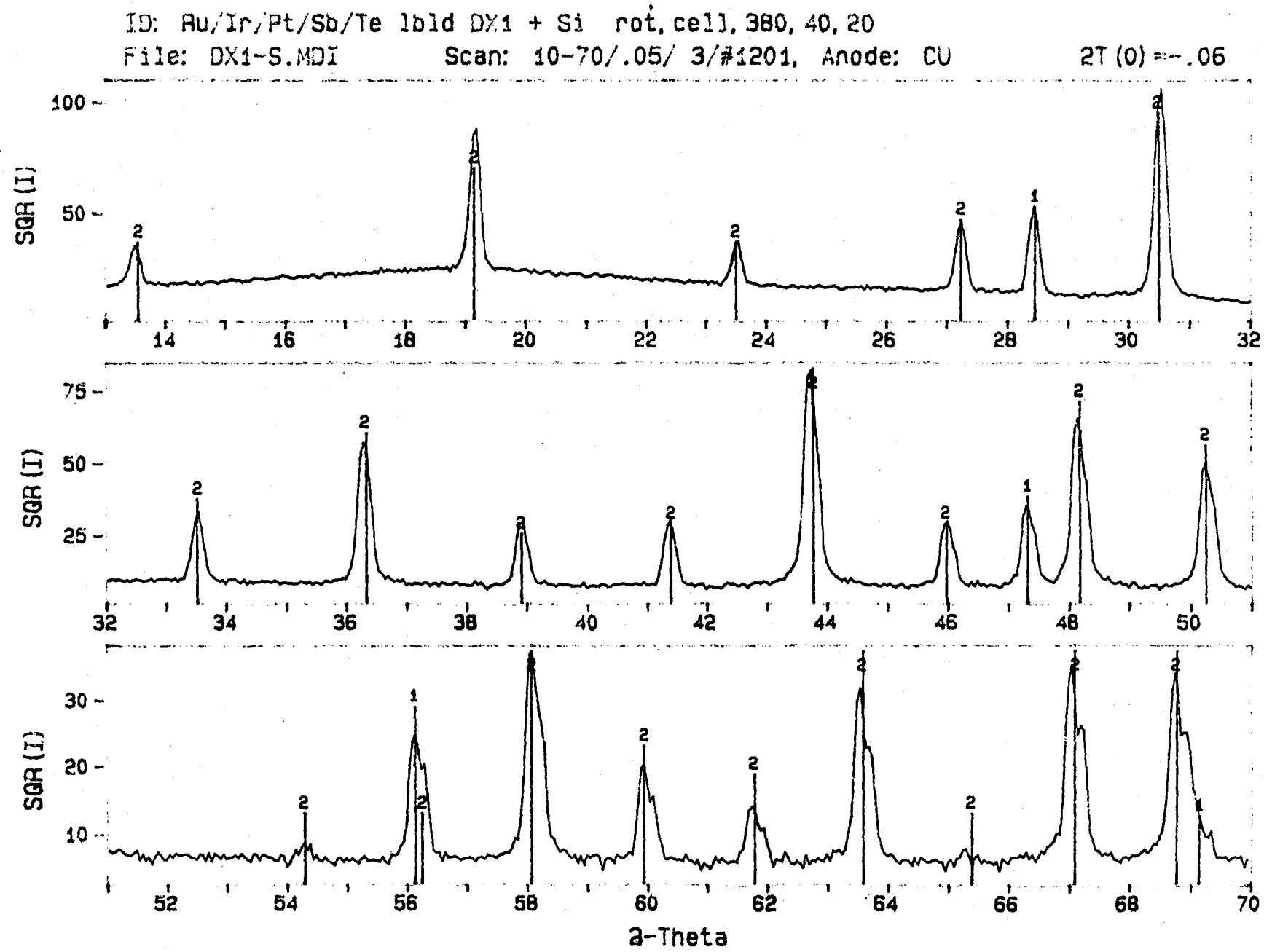
ID: Au/Ir/Pt/Sb/Te 1bld DX1 + Si rot, cell, 380, 40, 20
File: DX1-S.MDI Scan: 10-70/.05/ 3/#1201, Anode: CU 2T(0) =-.06
SQR(I)
100
50
14
16
18
20
22
24
26
28
30
32
SQR(I)
75
50
25
32
34
36
38
40
42
44
46
48
50
SQR(I)
30
20
10
52
54
56
58
60
62
64
66
68
70
2-Theta
1> 27-1402: Silicon, syn - Si
2> P17-0888 Ir Sb3, d/d(0)=1.0007

Figure 11

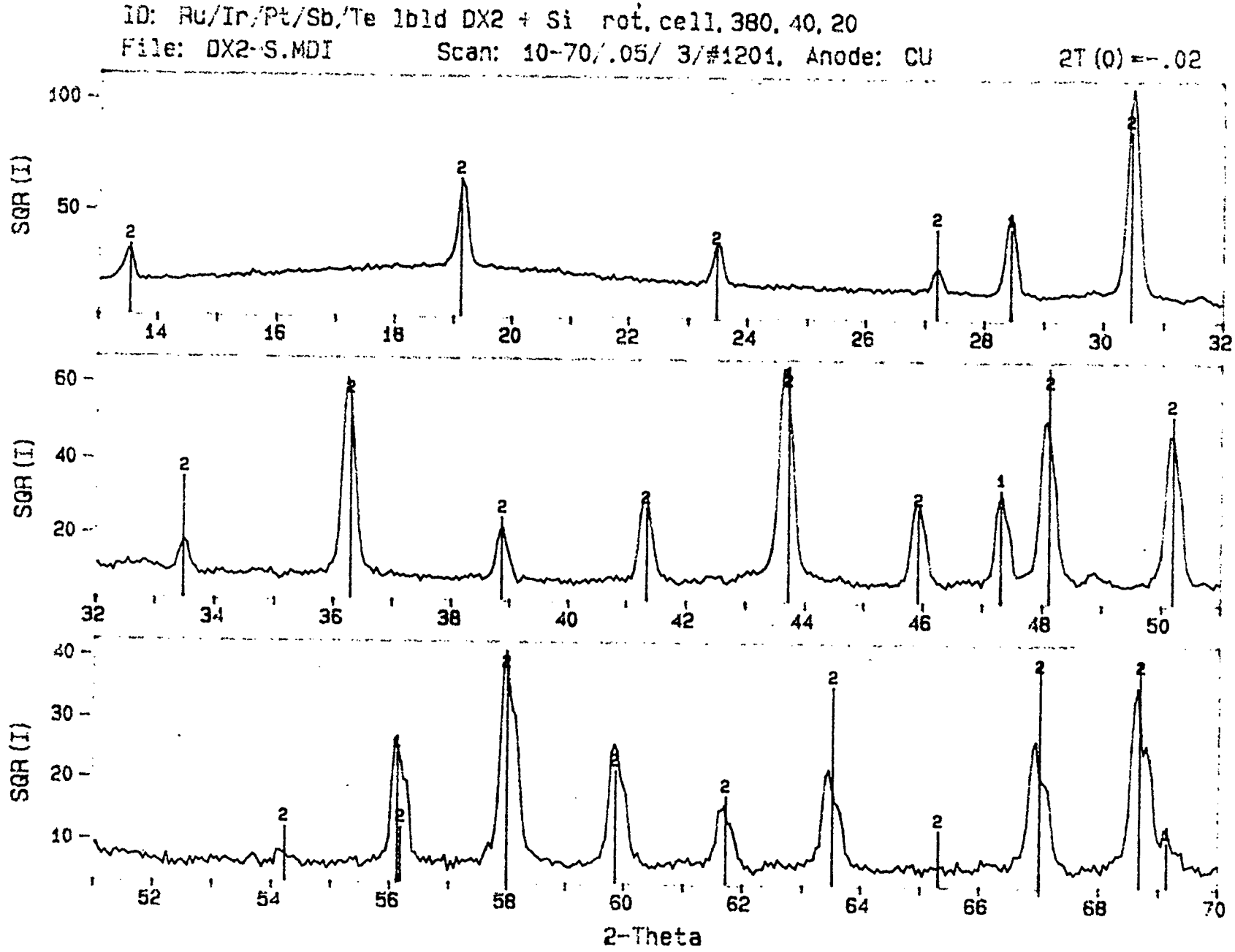
ID: Ru/Ir/Pt/Sb/Te 1bld DX2 + Si rot. cell. 380. 40. 20
File: DX2-S.MDI Scan: 10-70/.05/ 3/#1201. Anode: CU
2T (0) =-.02
SQR (I)
2-Theta
1> 27-1402: Silicon, syn - Si
2> P17-0888 Ir Sb3, d/d (0) =1.0018

Figure 12

DX-2

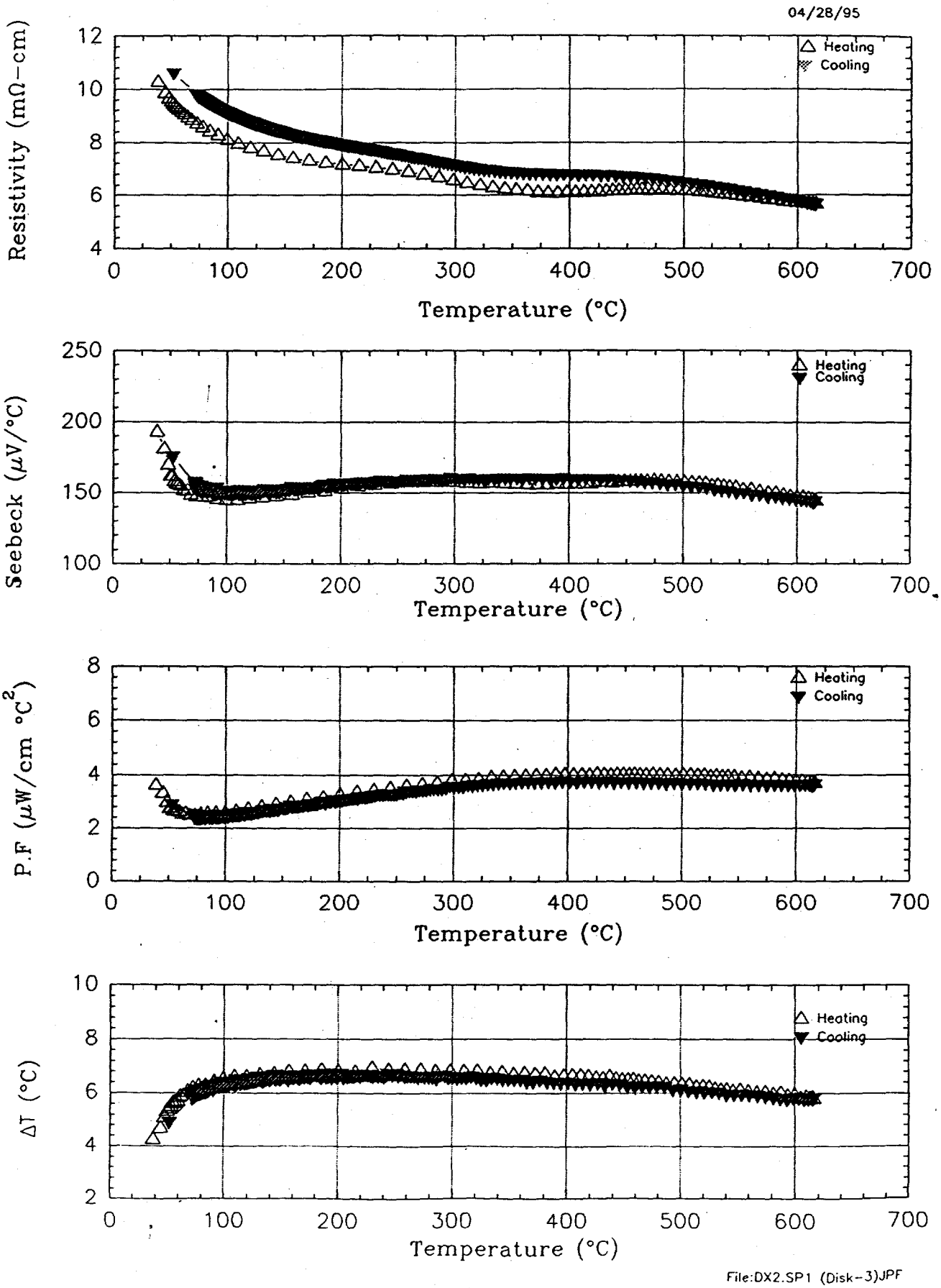

Figure 13

DX1

04/27/95

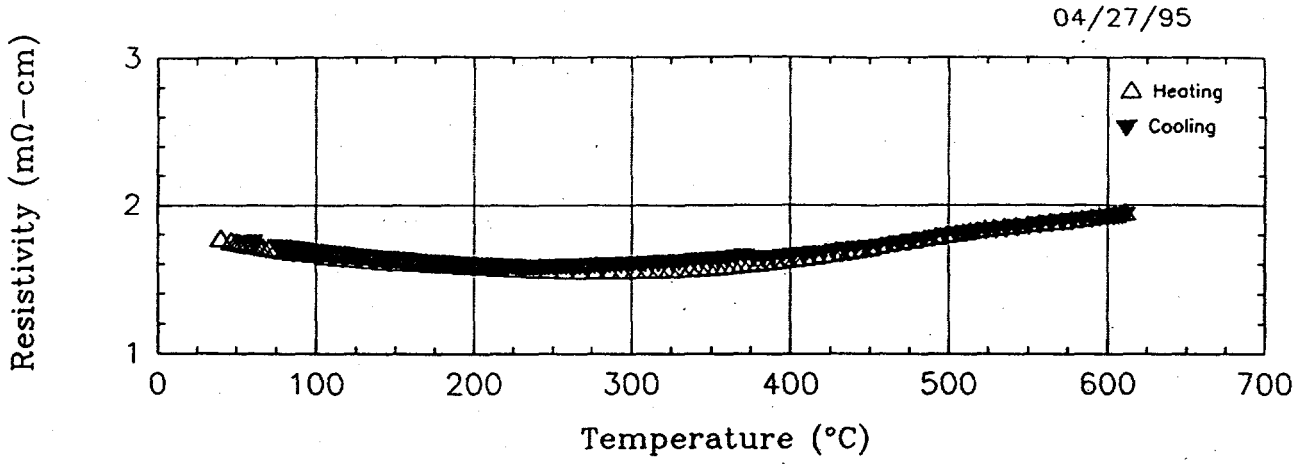

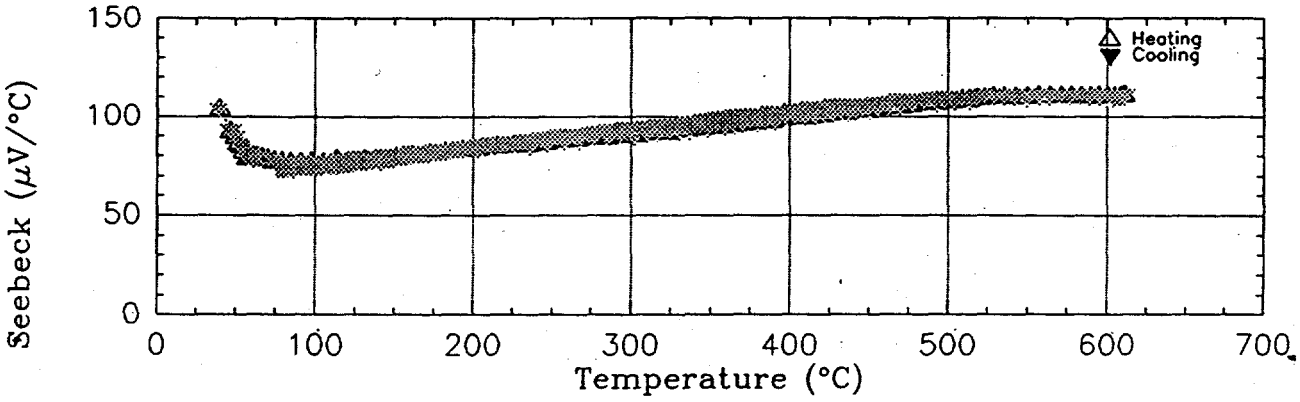

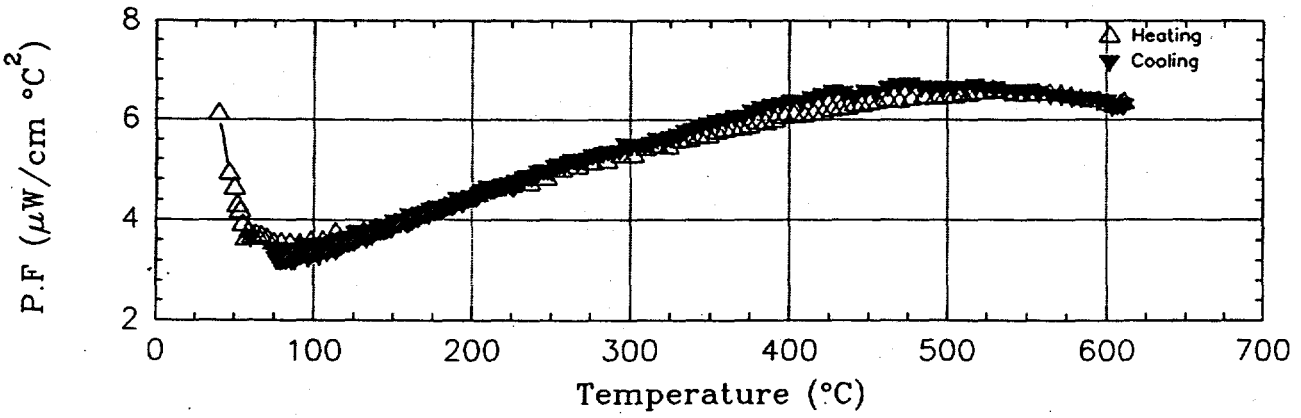

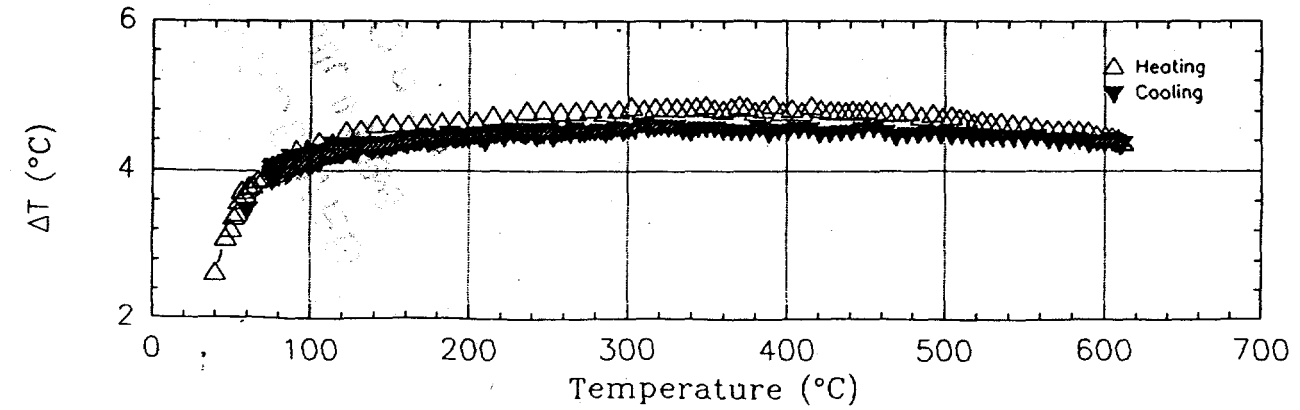

File:DX1.SP1(Disk-3)JPF.